ELSEVIER

Contents lists available at ScienceDirect

### Journal of Magnetic Resonance

journal homepage: www.elsevier.com/locate/jmr



# "Store-bought is fine": Sensitivity considerations using shaped pulses for DEER measurements on Cu(II) labels



Joshua Casto, Xiaowei Bogetti, Hannah R. Hunter, Zikri Hasanbasri, Sunil Saxena\*

Department of Chemistry, University of Pittsburgh, Pittsburgh, PA 15260, United States

#### ARTICLE INFO

Article history: Received 21 November 2022 Revised 27 January 2023 Accepted 22 February 2023 Available online 26 February 2023

Keywords:
DEER
Spin-labeling
Pulse shaping
EPR
Paramagnetic spins

### ABSTRACT

The narrow excitation bandwidth of monochromic pulses is a sensitivity limitation for pulsed dipolar spectroscopy on Cu(II)-based measurements. In response, frequency-swept pulses with large excitation bandwidths have been adopted to probe a greater range of the EPR spectrum. However, much of the work utilizing frequency-swept pulses in Cu(II) distance measurements has been carried out on home-built spectrometers and equipment. Herein, we carry out systematic Cu(II) based distance measurements to demonstrate the capability of chirp pulses on commercial instrumentation. More importantly we delineate sensitivity considerations under acquisition schemes that are necessary for robust distance measurements using Cu(II) labels for proteins. We show that a 200 MHz sweeping bandwidth chirp pulse can improve the sensitivity of long-range distance measurements by factors of three to four. The sensitivity of short-range distances only increases slightly due to special considerations for the chirp pulse duration relative to the period length of the modulated dipolar signal. Enhancements in sensitivity also dramatically reduce measurement collection times enabling rapid collection of orientationally averaged Cu(II) distance measurements in under two hours.

© 2023 Elsevier Inc. All rights reserved.

### 1. Background

Electron paramagnetic resonance (EPR) has become an invaluable methodology in the field of structural biology and biophysics [1,2]. Pulsed EPR techniques [3–8] offer a robust means to measure 2–16 nm range distance constraints [9] between specific residues in proteins [10] or nucleic acids [11]. The monitoring of these distance constraints can provide fundamental insight on induced conformational changes [12–15], biomolecular interactions [16–20], substrate and cofactor coordination [21–24], equilibrium constants and properties [25–27], and quaternary structure [28–32]. Additionally, Continuous Wave EPR (CW-EPR) is commonly utilized to probe site-specific dynamics of biomolecules by observing changes in the EPR spectra [33–35].

Since most biomolecules lack native unpaired electrons, the EPR active sites are strategically engineered into a biomolecule through site-directed spin labeling methodology [36,37]. Traditionally, spin labels based on nitroxide radicals [38–40] have been primarily used in these measurements. Over the last decade, new classes of spin labels have emerged to expand the range of biological applications. In particular, Gd(III) based labels [41,42] have had an impact

\* Corresponding author. E-mail address: sksaxena@pitt.edu (S. Saxena). on in-cell distance measurements [43,44]. Carbon radicals [45–48] have also been developed to strengthen the application of EPR to in-cell measurements. Finally, Cu(II) based protein and DNA labels are incisive probes of backbone conformations and dynamics.

The EPR spectra of paramagnetic metal spins are GHz broader than that of nitroxide [49]. For example, at X-Band ( $\sim$ 9.6 GHz) distorted octahedral coordinated Cu(II) spins [50] have an approximately 1.8 GHz wide spectrum due to the large intrinsic ganisotropies and hyperfine splitting. On the other hand, nitroxides have an EPR spectrum that is ~250 MHz wide. When operating at Q-Band (~34 GHz), the spectral effects of g-anisotropies further increase resulting in a Cu(II) spectral width of  ${\sim}5$  GHz. Pulsed experiments, such as Double Electron-Electron Resonance (DEER) [51], traditionally utilize rectangular monochromic pulses with excitation bandwidths between ~40–100 MHz. Rectangular pulses can excite a substantial portion of the nitroxide EPR spectrum, but their finite bandwidths excite only a narrow portion of the Cu(II) spectrum. However, Cu(II) measurements are often performed at low temperatures which increases spin polarization and mitigates somewhat the loss of signal due to limited excitation. The excitation of a smaller sub-set of spins compared to nitroxides can also lead to other complications for distance measurements.

For Cu(II) protein labels, narrow pulse bandwidths probe only a subset of molecular orientations at Q-Band [52]. This orientational

selectivity effect has been exploited to determine protein subunit orientation to add another structural dimension to distance constraints [53]. Nevertheless, additional measurements at different magnetic fields are then required to mitigate orientational selectivity and obtain accurate distance distributions. Carrying out multiple measurements increases the collection time necessary to measure a distance.

In response to these concerns, shaped frequency-swept pulses generated using arbitrary waveform generators (AWG) [54,55] have come into focus for EPR measurements [56–59]. Shaped pulses are advantageous since they can excite a greater range of the EPR spectrum [60]. One example is the chirp pulse that sweeps a range of frequencies over the pulse duration [56,61]. Additionally, chirp pulses excite spins more uniformly over the bandwidth in contrast to the sinc-shaped excitation profiles of rectangular pulses. To this end, frequency-swept pulses have recently been incorporated in distance measurements between paramagnetic spins to increase sensitivity [62].

However, much of the work done utilizing frequency-swept pulses for distance measurements has been done with nitroxides [63,64] and Gd(III) [65]. For Cu(II), sensitivity improvements from frequency-swept pulses have largely been demonstrated with home-built spectrometers, ultra-wide band (≥500 MHz) pulses [60], loop gap resonators [66], and for ESEEM [67] and Relaxation Induced Dipolar Modulation Enhancements (RIDME) measurements [68].

In this work we outline the use of frequency-swept pump pulses in DEER measurements with a focus on Cu(II)-based spin labels for DNA and proteins [69]. Herein we make comparative measurements at X and Q-Band frequencies. More importantly, Q-Band DEER measurements on Cu(II) labeled proteins necessitate specialized acquisition schemes to mitigate orientational effects [52]. Therefore, a systematic examination and improvement of sensitivity for this label is important to promote the widespread use of this technology.

### 2. Materials and methods

### 2.1. hGSTA1-1 preparation

The K211H/E215H human Glutathione S-Transferase (hGSTA1-1) mutant was expressed in E. coli BL21(DE3) cells as described before [70]. The protein expression was induced with 500  $\mu$ M Isopropyl  $\beta$ -D-1-thiogalactopyranoside for 4 h after reaching an  $OD_{600} = 0.6-0.8$ . A two-step purification was first carried out through HiTrap Q HP anion exchange column, then the fraction containing the hGSTA1-1 was further purified through GFC sizeexclusion column. The purified protein was concentrated in pH 6.5 50 mM sodium phosphate buffer with 150 mM NaCl, aliquoted and stored at -80 °C. To prepare the EPR samples, a 10 mM Cu(II)-NTA stock was first made using previously described protocols prepared **EPR** samples were [71]. All in morpholinopropanesulfonic acid (MOPS) buffer to facilitate Cu(II) coordination to two histidine sites [72]. The bound hGSTA1-1 samples contained 75 μM protein and 150 μM Cu(II)-NTA to saturate both dHis sites, one on each hGSTA1-1 subunit. Next, 200 µM of S-hexylglutathione (GSHex, purchased from Sigma Aldrich) was added to induce the liganded state of hGSTA1-1. Additionally, 40 % (v/v) d<sub>8</sub> glycerol was added as a cryoprotectant [73]. Final samples were prepared in pH 7.4 50 mM MOPS buffer and 100 mM NaCl with D<sub>2</sub>O as the solvent. All EPR samples were incubated at 4 °C for 35 mins to maximize Cu<sup>2+</sup>-NTA coordination [72]. Samples were placed in 2 mm I.D. 3 mm O.D. and 3 mm I.D. and 4 mm O.D. quartz tubes for Q-Band and X-Band measurements respectively. The samples were then transferred on ice to be immediately flash

frozen in liquid methylacetylene-propadiene propane (MAPP) gas [74].

### 2.2. GB1 preparation

All samples of immunoglobulin binding domain of protein G (GB1) used for experiments were mutated at sites E15H/T17H/ K28H/Q32H to create two dHis sites. The GB1 mutant plasmid was purchased from Synbio Technologies. GB1 expression and purification were performed using standard procedures in BL-21 E. coli cells [75,76]. The GB1 stock was prepared in 150 mM NaCl, 50 mM pH 6.5 sodium phosphate buffer, and 20 % glycerol (v/v) before being stored at -80 °C. Frozen GB1 was thawed on ice then passed through five HiTrap 5 mL desalting columns into pH 6.5 50 mM sodium phosphate buffer with 150 mM NaCl, before preparation. GB1 was then buffer exchanged with 50 mM of pH 7.4 MOPS buffer prepared in D<sub>2</sub>O. Final GB1 samples were prepared in 50 mM of pH 7.4 MOPS buffer, with a 1:1 M ratio of 75  $\mu$ M Cu<sup>2+</sup>-NTA per dHis site and refrigerated at 4 °C for 35 mins to maximize Cu<sup>2+</sup>-NTA coordination [72]. Next, 40 % (v/v) d<sub>8</sub> glycerol was added as a cryoprotectant. Samples were then transferred on ice to be immediately flash frozen in liquid MAPP gas after being placed in 2 mm I.D. 3 mm O.D. and 3 mm I.D. and 4 mm O.D. quartz tubes for Q-Band and X-Band measurements respectively [74].

### 2.3. Cu(II) labeling of DNA

Single-strand oligonucleotides (5'-TTG ACC TT(X) CCC CTT GCT GGA AGG TT(Z) TAA CCT-3' and 3'-AAC TGG AA(Z) GGG GAA CGA CCT TCC AA(X) ATT GGA-5') containing 2,2'-dipicolylamine (X) and an abasic site (Z) were obtained from Karebay Biochem Inc. The supplier purified the strands using HPLC and characterized them using mass spectrometry. Complementary DNA strands were mixed in addition to 1.25:1 equivalent of CuCl<sub>2</sub> per DPA to ensure coordination of DPA sites. Sample solutions were then annealed in D<sub>2</sub>O to increase Cu(II) chelation. Annealing was done by heating the samples to 90 °C for one minute, 60 °C for three minutes. 50 °C for five minutes. 40 °C for ten minutes. 30 °C for five minutes. and then cooled to 4 °C using a GeneAMP PCR System 9700. Final Cu(II) labeled DNA samples were prepared to 75 µM duplex and 150 μM Cu(II) in pH 7.4 50 mM NEM with 40 % (v/v) d<sub>8</sub> glycerol in D<sub>2</sub>O. The samples were then transferred on ice to be immediately flash frozen in liquid MAPP gas after being placed in 2 mm I.D. 3 mm O.D. and 3 mm I.D. and 4 mm O.D. quartz tubes for Q-Band and X-Band measurements, respectively.

#### 2.4. EPR experiments

Continuous Wave (CW) EPR experiments were performed to determine Cu(II) and Cu(II)-NTA coordination to DPA and dHis sites respectively. CW-EPR experiments were performed with a Bruker E580 X-Band (~9.4 GHz) FT/CW spectrometer with a Bruker ER4118X-MD5 resonator. Each spectrum was acquired at 80 K and contained 1024 data points, with a magnetic field sweep of 2000 G centered at 3100 G, 10.24 ns time constant, 20.48 ms conversion time, 100 kHz modulation frequency, a 4 G modulation amplitude, and an attenuation of 30 dB. The spectra were simulated and fit using the EasySpin software [77].

Pump pulse excitation profiles were obtained by first determining optimal observer pulse lengths in 10 MHz intervals  $\pm$  150 MHz outside the MD5 central resonator frequency as described in previous literature [60]. Pulse lengths in the Hahn echo sequence were increased by 2 ns over 250 ns to determine the length for maximum echo inversion. Longitudinal magnetization was measured at each frequency interval by taking the ratio of the echo obtained with an inversion pulse at 0 and 100 amplitude added to the begin-

ning of the Hahn echo sequence. The rectangular 24 ns pump pulse was applied at the central frequency and chirp pump pulses were applied  $\pm$  100 MHz around the central frequency.

Q-Band frequency (~35 GHz) pulsed EPR experiments for distance measurements were performed using a Bruker E580 FT/CW spectrometer, 300 W TWT amplifier, ER5106-QT2 resonator, Bruker SpinJet AWG, and Bruker B8692690 cryogen free cryostat at 18 ± 1 K. The X-Band frequency pulsed EPR experiments for distance measurements were performed using a 1 kW TWT amplifier and Bruker ER4118X-MD5 resonator. The four-pulse Double Electron-Electron Resonance (DEER) sequence  $\left[ \left( \frac{\pi}{2} \right)_{\nu 1} - \tau_1 - (\pi)_{\nu 1} - (\tau_1 + T) - (\pi)_{\nu 2} - (\tau_2 - T) - \pi_{\nu 1} - \tau_2 - echo \right]$ with 16 step phase cycling [6] was used. For all samples, the observer pulses,  $(\frac{\pi}{2})_{v1}$  and  $\pi_{v1}$ , were determined to be 10 and 20 ns, respectively. The pump pulse,  $(\pi)_{v^2}$ , was set to either 24 ns rectangular, or 64/100/240 ns chirp with a frequency range from -300 to -100 MHz relative to the observer frequency. Shaped pulses were generated with the 1.6 GS/s Bruker SpintJet AWG have a 14 bit amplitude resolution, 0.625 ns time resolution, and ±400 MHz around the carrier frequency. The pump pulse was stepped out by 30 ns for 253 points over T, to achieve a maximum dipolar evolution time of 7.6 µs for hGSTA1-1 and DNA samples. For measurements on GB1, the pump pulse was stepped out by 8 ns for 157 points over T, to achieve a dipolar evolution time of 1.2 us. The pump pulse was applied at the magnetic field corresponding to the greatest intensity determined by an echo detected field sweep. All measurements were obtained with 20 shots per data point and a 1500 µs shot repetition time between data point collections. All DEER time traces were collected with the VAMP (Video AMPlifier) maximum video bandwidth set to 20 MHz. The echo integrator gate length was set as the full width at half max of the DEER echo. Integrator gate lengths varied between ~50-64 ns depending on operating frequency and magnetic field position of the measurement. DEERNet [78] and DEERAnalysis 2019 [79] software packages were used to determine the distance distributions.

#### 3. Results and discussion

3.1. Lack of orientational selectivity makes DNA Cu(II) labels ideal for sensitivity comparisons

First, we carried out DEER distance measurements on a DNA duplex spin labeled with Cu(II) [80]. A 31-base pair (bp) DNA duplex was purchased with 2,2-dipicolyamine (DPA) moieties and complementary abasic sites substituted into the duplex with an 18 bp separation. Next, DNA was labeled with Cu(II) as described in the Methods section. Fig. 1 shows the DNA sequence used in this work and the DPA moieties in the duplex after Cu(II) labeling. CW-EPR experiments, presented in Fig. S1 in the S.I., were then carried out to ensure DPA sites were sufficiently loaded with Cu(II) prior to distance measurements. All biomolecule and Cu(II) spin concentrations throughout this work were prepared to 75 and 150  $\mu$ M, respectively, for consistent comparison.

As highlighted in Fig. 1, the DPA moiety is attached to the backbone of the duplex by a short C-C-N linker (yellow). Molecular Dynamics (MD) simulations [81] have shown that the short linker positions the Cu(II) label inside the helix with the DPA moiety oriented similarly to natural bases. The placement of the label inside the duplex close to the backbone provides Cu(II)-Cu(II) distances within 0.1–0.2 nm of the C4'-C4' duplex backbone distance [82].

In addition, the three Cu(II)-N bonds are elastic and have a range of bond lengths and bond dihedral angles. Each DNA, therefore, might contain Cu(II) labels with slightly different bond angles and lengths in the frozen ensemble. Thus, there exists a range of *g*-tensor orientations between Cu(II) spins in the ensemble. Fig. 1 depicts the *g*-tensor orientations of a spin pair as purple arrows for spin A and blue arrows for spin B. The dashed grey angles  $\chi$ ,  $\eta$ , and  $\gamma$  defined in Fig. 1 are used to characterize the orientations between the spins and  $\overrightarrow{r}$  [83]. These angles can have a standard deviation of approximately 25° [81]. The contributions from the flexible DPA linker increases the standard deviation of the angles in Fig. 1 close to 70° [81].

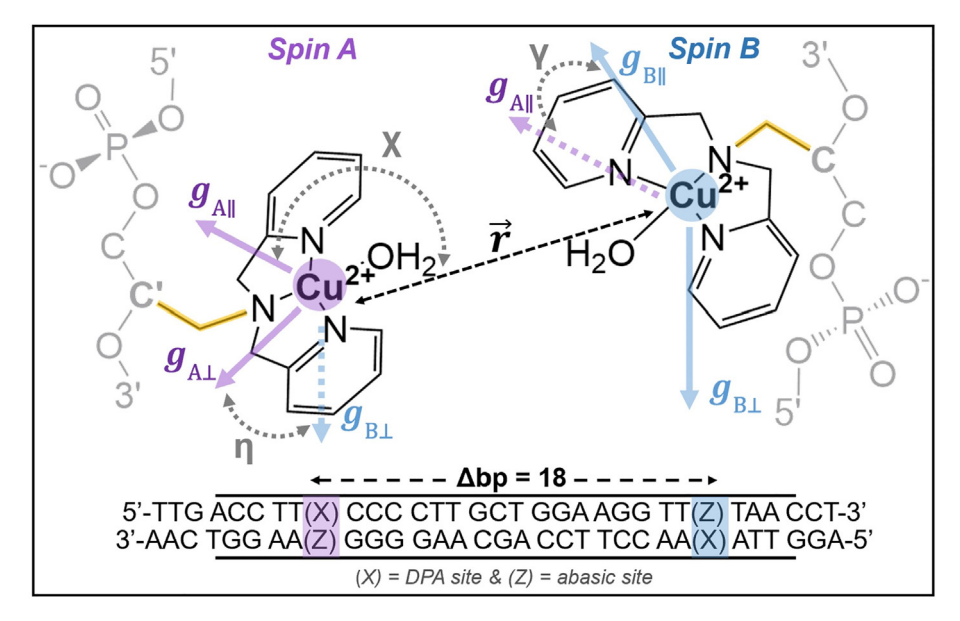


**Fig. 1.** A) Cartoon representation DPA (grey) moieties coordinated with Cu(II) on opposing duplex strands. The black dashed line represents the interspin vector,  $\vec{r}$ , between the Cu(II) spin centers. The relative orientations of the spin labels are depicted by the grey arrows for three angles  $\chi$ ,  $\eta$ , and  $\gamma$ . The bonds highlighted in yellow are the linker between the DPA and DNA backbone. The DNA sequence is shown at the bottom. (X) indicates DPA sites and (2) indicates the complementary abasic site. (For interpretation of the references to colour in this figure legend, the reader is referred to the web version of this article.)

Such variation in **g**-tensor between Cu(II) in the ensemble produces a large orientational distribution of the spins. In return this label does not have orientational selectivity effects in DEER at either X or Q-Band frequencies. The lack of orientational selectivity has also been demonstrated experimentally [80,82]. Therefore, this spin label is an ideal system to directly compare the sensitivity of commercial frequency-swept pulses to monochromic rectangular pulses for Cu(II) spin labels.

### 3.2. Commercial chirp pulses have uniform spin excitation compared to rectangular pulses

We performed our comparative DEER experiments using rectangular and frequency-swept pulses. The pump pulses used in this work are a 24 ns monochromic rectangular pulse and a 250 ns chirp pulse with a 200 MHz frequency-swept bandwidth at both X and Q-Band, unless otherwise stated. The rectangular pulse was determined to be 24 ns from a pulse length nutation performed at the Q-Band experimental frequency (Fig. S2). With the 300 W TWT at Q-Band and QT2 resonator, a 24 ns rectangular pulse was the shortest pulse length that we were able to obtain. For this reason, X-Band experiments were also performed with a 24 ns pulse for a direct comparison to Q-Band, even though pulse lengths as short as 16 ns have been achieved with the X-Band MD5 resonator [82] (c.f. Fig. S2).

The chirp pulse was set to 200 MHz to maximize the bandwidth of the pump pulse while also staying within the resonator bandwidth of  $\sim\!\!300$  MHz when using a 100 MHz offset between the observer and pump pulses. Such an offset is necessary to mitigate pulse overlap and the contribution of nuclear hyperfine interaction to the DEER signal for Cu(II) spin labels at X-Band. Further, the total 300 MHz observer and pump pulse frequency offset is within the  $\pm$  400 MHz bandwidth of the Bruker Spin-Jet AWG around the operational frequency.

Fig. 2A depicts the idealized uniform spin excitation profile of chirp pulses compared to rectangular. These spin profiles were calculated with EasySpin [77] software using a general two spin state system. Here, the y-axis  $\rm M_z/\rm M_0$  is the ratio of the longitudinal spin magnetization after the pump pulse,  $\rm M_z$ , to the magnetization at equilibrium,  $\rm M_o$ . The frequencies where  $\rm M_z/\rm M_0$  equals -1 suggests a complete spin flip with the pump pulse. In reality, the experimental inversion profiles differ from the simulated due to hard-

ware limitations that perturb the adiabaticity of the shaped pulse and the linearity of coherence transfer [56,61]. Fig. 2B shows how our experimental spin excitation profiles using our MD5 resonator indeed differ from the ideal case. Note that methodology to manipulate the initial pulses in order to generate more uniform excitation has been reported [57,61].

### 3.3. Commercial chirp pulses provide significant sensitivity gains for *Cu(II)* spin pairs

Fig. 3 shows the 4 Pulse DEER scheme used throughout this work. The measured DEER signal is the stimulated DEER echo depicted in black. Fig. 3 also shows that the Q-Band DEER echo acquired at a 5 μs dipolar evolution time for Cu(II) labeled DNA samples is one magnitude higher in SNR than the echo at the same dipolar evolution time for X-Band. This difference in echo magnitude is anticipated given prior work on nitroxides [84]. The higher frequency of Q-Band increases the energy level difference between the excited and ground states resulting in greater spin polarization than X-Band [84,85]. Additionally, the sample volumes used for Q-Band measurements are often smaller than X-Band. Having a smaller ratio of resonator volume to sample volume increases the resonator filling factor to better store incident microwave [66]. Cumulatively these attributes provide significant increases to sensitivity.

Fig. 4 shows the background subtracted DEER signal of the DNA at both X and Q-Band. The raw DEER data are presented in Fig. S3 in the S.I. Time traces presented in this work were collected until a desired signal to noise (SNR) ratio was reached unless otherwise stated. The SNR and other relevant sensitivity data for all distance measurements discussed throughout this work are presented in the SI (c.f. Tables S1 and S2). To make sensitivity comparisons, we evaluated the modulation depths ( $\lambda$ ) of the data. As depicted in Fig. 4A,  $\lambda$  is the difference in intensity between the zero time and the end of the background subtracted time trace (black dashed line). This parameter is dependent on the percent of spin pairs that are excited by the pump pulse in DEER [86]. Herein we used a criteria for the sensitivity (SNR) of a DEER measurement as defined previously [87]:

$$SNR \approx \frac{\lambda}{\sigma_{Noise}} \tag{1}$$

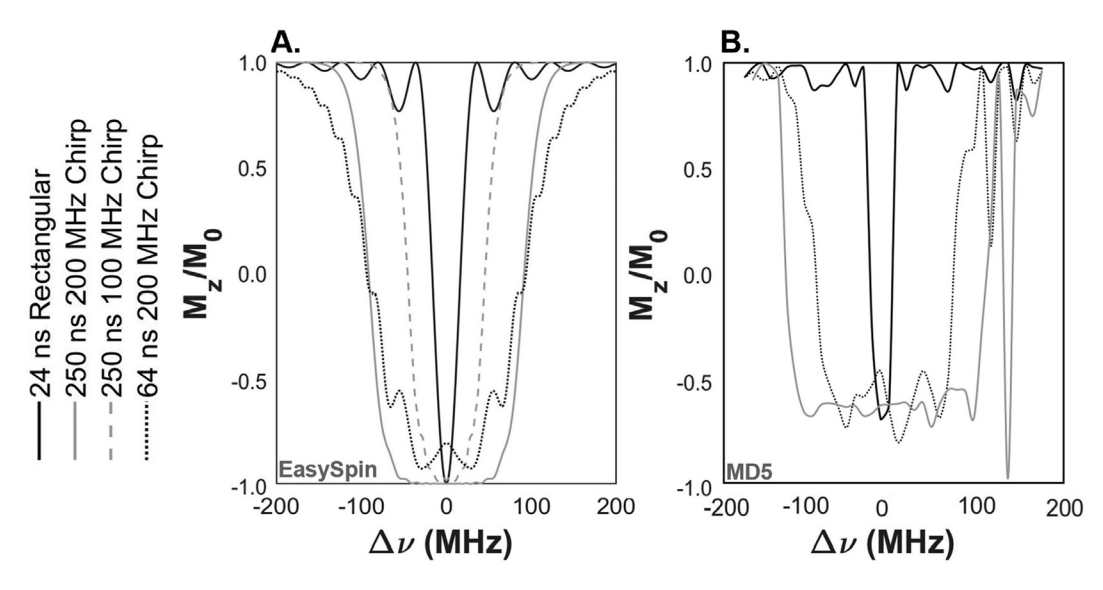
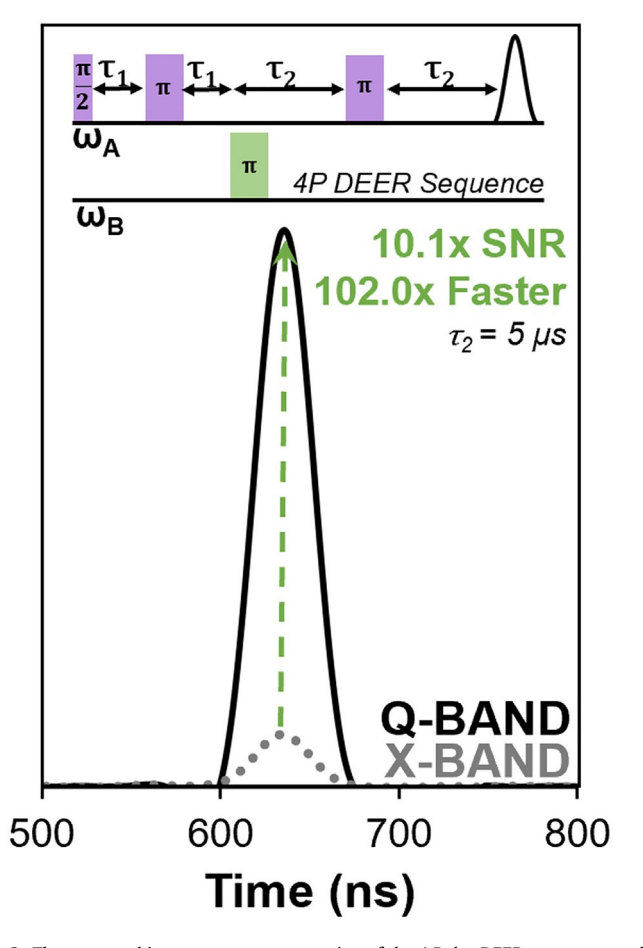


Fig. 2. A) DEER pump pulse spin inversion profiles for each pump pulse type as described. Profile spin inversions were simulated using EasySpin in MATLAB R2020b. B) Experimentally measured pump pulse spin inversion profiles of the different pulse types collected using the X-Band MD5 resonator.



**Fig. 3.** The top panel is a cartoon representation of the 4 Pulse DEER sequence used in this work. Below the pulse sequence is a comparison between Q-Band (black solid) and X-Band (grey dotted) DEER stimulated echoes at a  $\tau_2=5~\mu s$  dipolar evolution time for DNA labeled with Cu(II). Both echoes were collected at the field of maximum absorption. Q-Band has one magnitude higher SNR than X-Band.

In Eq (1),  $\sigma_{\text{Noise}}$  is the root mean square deviation (RMSD) of the noise. As done in previous literature,  $\sigma_{\text{Noise}}$  was calculated by dividing the background subtracted DEER by the DEERAnalysis fit to isolate the noise signal [87]. The RMSD of the noise was then calculated for each measurement to obtain  $\sigma_{\text{Noise.}}$  Further, the rectangular pulse provides a  $\lambda$  of 2.6 % at Q-Band. This  $\lambda$  agrees with theoretical calculations based on the Field Swept Electron Spin Echo (FS-ESE) spectrum detailed in the S.I. (Fig. S4). Upon incorporation of the optimal chirp pump pulse the  $\lambda$  increases significantly by a factor of three. This result is expected since the spin inversion profile of chirp pulses are more homogenously uniform across the bandwidth of the chirp pulse bandwidth than the rectangular pulse (cf. Fig. 2). Previous work that employed ultra-wide band frequency-swept pulses (>500 MHz) using a commercial spectrometer and  $TE_{102}$  Box resonator reported a  $\lambda$  of 3 % [60]. When using a loop gap resonator with the same ultra-wide band pulse. a  $\lambda$  of 12 % was obtained. Indeed, the chirp pulse we used provided sensitivities that are on par with those achieved with ultra-wide band pulses and home-built resonators. Thus, these results suggest that dramatic improvements of SNR on commercial equipment are possible.

Next, similar DEER measurements were performed at X-Band. Fig. 4B shows that chirp pump pulses provide significant increases in sensitivity at X-Band as well. Fig. 4C shows the FS-ESE spectra at both X and Q-Band. The narrower spectral width at X-Band leads to a higher  $\lambda$  than Q-Band using the same pump pulse, since the chirp pulse, represented by purple bar in Fig. 4C, excites a greater percentage of the total spins. Improvements may be possible by increasing the sweep bandwidths using ultra-wide band pulses. Even though these results were obtained on DNA labels, we anticipate similar results for measurements on other Cu(II) systems that lack orientational selectivity.

These X-Band results are exciting since Q-Band is not accessible to everyone who utilizes pulsed EPR techniques. Additionally, this increase in sensitivity at X-Band is significant for those who may want to circumvent orientational selectivity effects for Cu(II) protein labels at Q-Band (cf. next section).

In contrast to our DEER results, RIDME measurements between Cu(II) spins using commercial spectrometers have provided  $\lambda$  up to

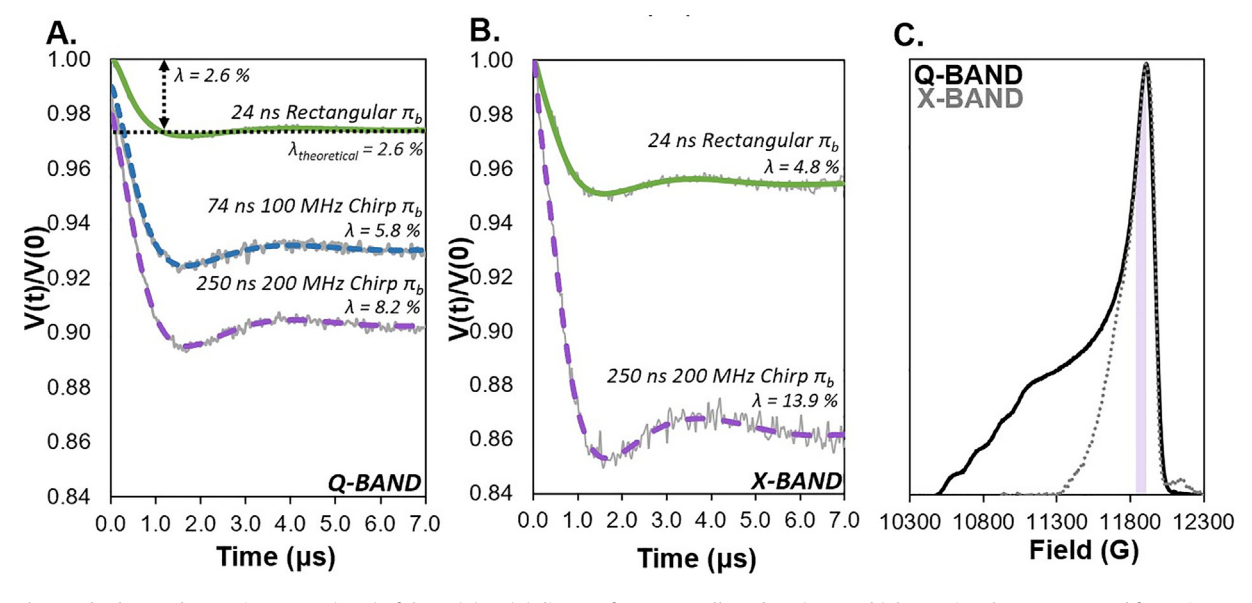


**Fig. 4.** Background subtracted DEER time traces (grey) of the Cu(II)-Cu(II) distance from DNA collected at A) Q-Band (The y-axis values are staggaed for easier comparison of the time traces) and B) X-Band. Time trace fits (green, blue, purple) were obtained by DEERAnalysis2019 via Tikhonov regularization. The pump pulse utilized for each time trace is shown. C) Comparison of Q-Band (black solid) and X-Band (grey dotted) DNA Cu(II) label Field Swept Electron Spin Echo. The x-axis for the X-Band data was shifted up-field for direct comparison to Q-Band data. The purple shaded region represents the range of excitation from a 250 ns 200 MHz pump pulse. (For interpretation of the references to colour in this figure legend, the reader is referred to the web version of this article.)

49 % with shaped pulses [60]. Since RIDME is a single frequency pulse technique, the method has also recently come into focus for orthogonal labeling schemes involving Cu(II) [88]. RIDME is especially useful for such measurements because using a single frequency makes the field separation between the orthogonal spin EPR spectra less relevant [65,68]. Notably, Cu(II)-nitroxide RIDME measurements have provided a pathway for distance measurements at nanomolar concentrations [25]. However, RIDME has a complex background signal that makes data analysis complicated [5]. In addition, the slope of the background signal limits the ceiling of measurable distances with RIDME [5]. Given that details on optimization experimental implementation of RIDME are available elsewhere [5,60], we have focused on DEER for this work.

### 3.4. Orientational selectivity acquisition schemes impacts sensitivity for Cu(II) protein labels

Next, we performed DEER measurements on the E211H/K215H hGSTA1-1 protein spin labeled with Cu(II). These experiments were performed in the presence of an S-alkyl glutathione inhibitor [89] derivative, GSHex, to induce the ordered active state conformation of hGSTA1-1. The structure of this liganded hGSTA1-1 complex has been well reported in both EPR measurements [70] and Xray crystallography [90], making it an ideal model system for longrange EPR distance measurements. Further, this hGSTA1-1 mutant is strategically designed so that it has two histidine mutations (dHis) at i and i + 4 positions to enable Cu(II) coordination to the  $\alpha$ -helix [91]. Fig. 5A shows a schematic of the dHis labeling scheme in hGSTA1-1. Since hGSTA1-1 is a homodimer, only one dHis site per monomer is necessary to provide two spin labeled sites for distance measurements. The dHis sites were labeled by using a Cu(II) nitrilotriacetic acid (NTA) complex [71]. Cu(II)-NTA has only two free equatorial coordination sites to ensure specific binding to dHis (Fig. 5A). Additionally, CW-EPR experiments were first done to validate sufficient coordination of Cu(II)-NTA and dHis before carrying out distance measurements (c.f. Fig. S5 in S.I.).

Notably, this Cu(II) label is small and provides distance distributions that are up to five times narrower than common nitroxides [92–94]. Additionally, the standard deviation is only  $\sim\!12^\circ$  for the orientation angles  $\chi,\,\eta,$  and  $\gamma$  (c.f. Fig. 1) [48,69]. Thus, there is a narrow orientational distributions of Cu(II) spins in the ensemble that causes orientational effects in DEER at Q-Band, but not at X-band [69]. In brief, the finite bandwidth of the pump pulse relative to the breadth of the Cu(II) FS-ESE spectrum only probes a subset of molecular orientations. Therefore, multiple DEER need to be performed throughout the Cu(II) spectrum at Q-band to sufficiently sample all spin orientations in order to obtain an orientationally averaged DEER and correct distance distribution.

Herein we adopted an efficient Q-Band DEER collection scheme that was recently developed to provide robust distance constraints using Cu(II) labels [95]. In this scheme data is collected by probing spins approximately 100 G, 540 G, and 830 G downfield from the field of maximum absorption. The summation of these three measurements properly samples a sub-ensemble of all orientations to ensure a correct distance distribution [95]. Fig. 5B shows the positions of the pump pulses (cf. purple lines) overlaid on FS-ESE spectrum. The drawback of this acquisition scheme is that measurements were performed downfield from the maximum of the Cu(II) FS-ESE spectrum. Fig. 5C shows the DEER echoes obtained at the different fields with a dipolar evolution time of 5 μs. The decrease in the echo intensity leads to a decrease in the DEER sensitivity. In addition, the modulation depth,  $\lambda$ , and DEER echo intensity are smaller in these measurements than those conducted at the maximum position. To partly remedy this loss of sensitivity, we explored the use of chirp pulses to enhance  $\lambda$ .

## 3.5. Chirp pulses significantly increase modulation depths for Cu(II) protein labels

Fig. 6A shows the background subtracted time traces obtained with the chirp pulse as an example of the orientational selectivity acquisition scheme. The raw DEER data at Q and X-Band are provided in the S.I. (c.f. Fig. S6A). Fig. 6A also exemplifies the decrease

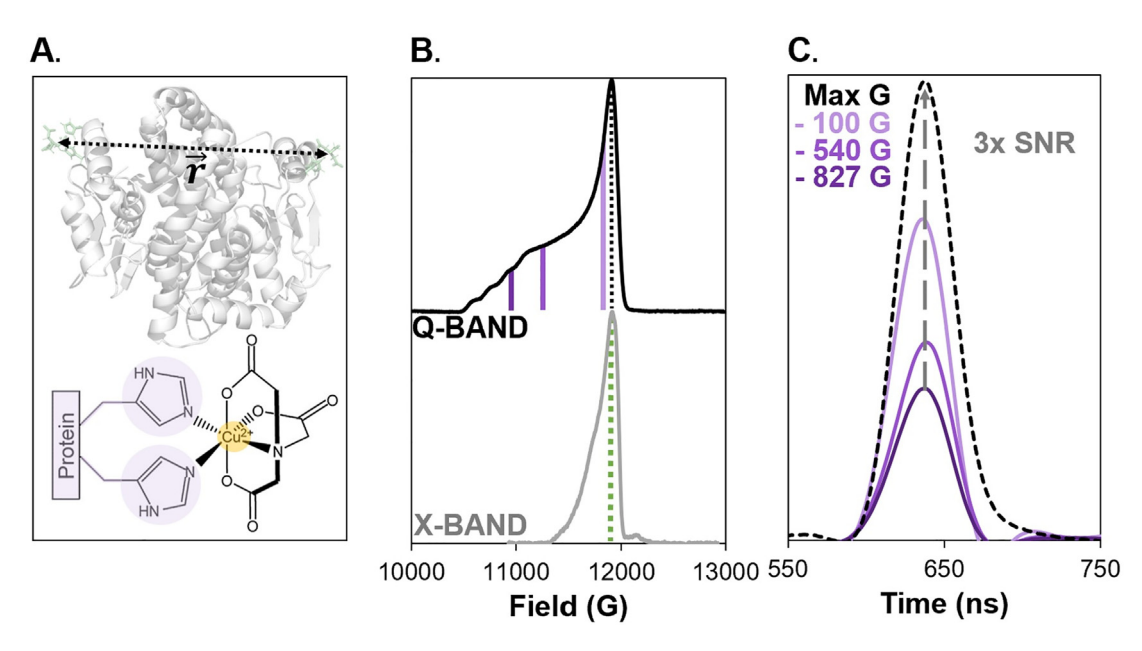


**Fig. 5.** A) Cartoon representation of E211H/K215H (green) hGSTA1-1 (grey) and the Cu(II) protein spin label motif. B) Comparison of Cu(II) field sweeps obtained at Q-Band (black solid) and grey (grey dotted). Purple lines indicate the fields at which Q-Band DEER measurements were collected, and the green line indicates the field probed at X-Band (note that the X-band data is shifted upfield for comparison). C) Comparison of Q-Band echoes obtained at the magnetic fields as described. The grey arrow exemplifies the difference in echo SNR between the lowest and maximum magnetic fields. Each echo was acquired at a dipolar evolution time of 5 μs. (For interpretation of the references to colour in this figure legend, the reader is referred to the web version of this article.)

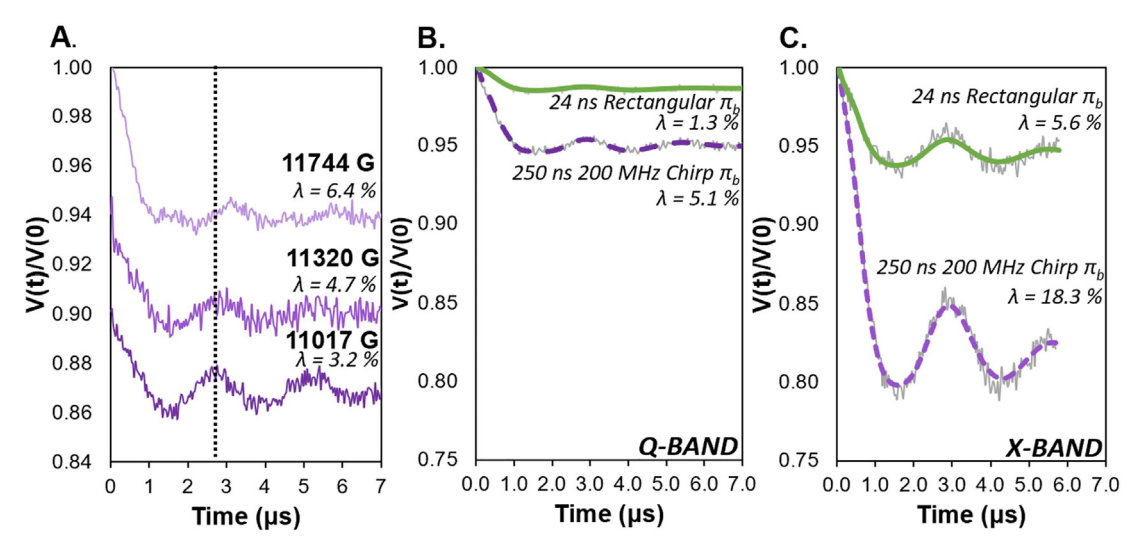


**Fig. 6.** A) Background corrected Q-Band signals at three fields for Cu(II) labeled hGSTA1-1. The y-axis values are staggered for easier comparison of the time traces. B) Summed orientationally averaged Q-Band time traces C) and DEER data at X-Band. Time trace fits (green, and purple) were obtained by DEERAnalysis2019 using Tikhonov regularization. The pump pulse utilized for each time trace is shown. (For interpretation of the references to colour in this figure legend, the reader is referred to the web version of this article.)

in  $\lambda$  as the magnetic field decreases. Additionally, the time traces show clear effects of orientational selectively. For example, the modulation period changes with magnetic field (cf. dashed line in Fig. 6A).

The individual traces were first normalized and then scaled with respect to field sweep intensity at the magnetic field they were obtained. Next, the scaled time traces were summed to produce an orientationally averaged DEER. The summed Q-Band DEER are presented in Fig. 6B. Although the  $\lambda$  are less than those obtained with Cu(II) DNA labels (c.f. Fig. 4A), the chirp pulses still increased the sensitivity by a factor of four. Indeed, orientationally selective measurements achieve  $\lambda$  that exceed previously reported  $\lambda$  obtained from commercial instrumentation [60].

Contrary to Q-Band measurements, the dHis motif is not orientational selective at X-Band [53]. Therefore, as shown in Fig. 5B, X-Band DEER were obtained by applying the pump pulses to the field of maximum absorption represented by the green dashed line. In Fig. 6C, we see the  $\lambda$  increase significantly upon using the chirp pulse. The results are encouraging because they demonstrate that modulation depths as much as ca. 18% can be readily achieved on commercial instrumentation.

### 3.6. Truncated chirp pulses for short-range distance measurements slightly improve sensitivity

So far, we have shown that commercial chirp pump pulses can provide significant increases to DEER sensitivities for Cu(II)-Cu(II) measurements regardless of the acquisition scheme. However, one of the primary limitations of frequency-swept pulses is the pulse length should not exceed one-fourth of the dipolar period [61]. The use of longer pulse lengths leads to an artificial broadening of the distance distribution. Therefore, short-range distances that have dipolar periods less than 1 µs cannot use the 250 ns chirp pulses. The simulated and experimental excitation profiles in Fig. 2A and Fig. 2B respectively show how shorter lengths for chirp pulses hinders the uniformity of excitation. Here we see that the 64 ns chirp pulse excitation profile has a smaller non-uniform inversion amplitude in addition to broader frequency flanks outside the designated bandwidth. Therefore, it is necessary to also examine how shorter chirp pulses explicitly affect the net sensitivity for short-range Cu(II)-Cu(II) DEER.

To this end we carried out distance measurements on a 15H/17H/28H/32H mutant of the immunoglobulin binding domain of protein G (GB1) spin labeled with Cu(II)-NTA. Distance measurements using dHis have been widely performed on this protein [72,96,97] with an expected distance distribution up to 2.5 nm. This distance corresponds to a dipolar period of approximately  $\sim$ 250 ns. To meet the duration restriction, we utilized a 64 ns chirp pulse. After spin labeling GB1, CW-EPR spectra were carried out to verify Cu(II)-NTA coordination to dHis prior to distance measurements (c.f. Fig. S5).

To properly sample orientations, three Q-Band DEER were obtained and then summed. The raw DEER traces are shown in Fig. S7 of the S.I. Fig. 7A shows background subtracted time traces for both pulse types. Here we see the chirp pulse slightly increases the sensitivity. However, this increase in sensitivity is less than those obtained with longer pulse lengths (c.f. Figs. 4 and 6). Fig. 7B also depicts a similar increase in sensitivity for short-range distance measurements at X-Band. These results were anticipated given the difference in spin excitation homogeneity depicted in Fig. 2. Regardless, the  $\lambda$  in Fig. 7A from the short chirp pulse remains on par with previously reported  $\lambda$  obtained with commercial instrumentation and ultra-wide band pulses [60].

Moreover, Fig. 7 depicts the Q-Band distance distributions for both pulse types are in excellent agreement.

### 3.7. Chirp pulses using commercial instrumentation provide sensitivities comparable with custom built equipment

Fig. 8 shows the  $\lambda$  from our measurements presented throughout this work. The  $\lambda$  reported from previous literature using a commercial spectrometer but different resonators and AWG [60] are shown as a comparison. The previous literature employed sixth order hyperbolic secant (HS6) shaped pump pulses. The HS6 pulse provides both a more uniform inversion profile over the designated bandwidth and preserves adiabaticity relative to chirp pulses [60]. We anticipate future incorporation of HS6 pulses with this spectrometer setup work will lead to further improvement in sensitivity.

Moreover, our  $\lambda$  obtained using the QT2 resonator exceeds  $\lambda$  from ultra-wide band pulses used with TE<sub>102</sub> box resonator. Since the observations in this work are primarily hardware dependent,

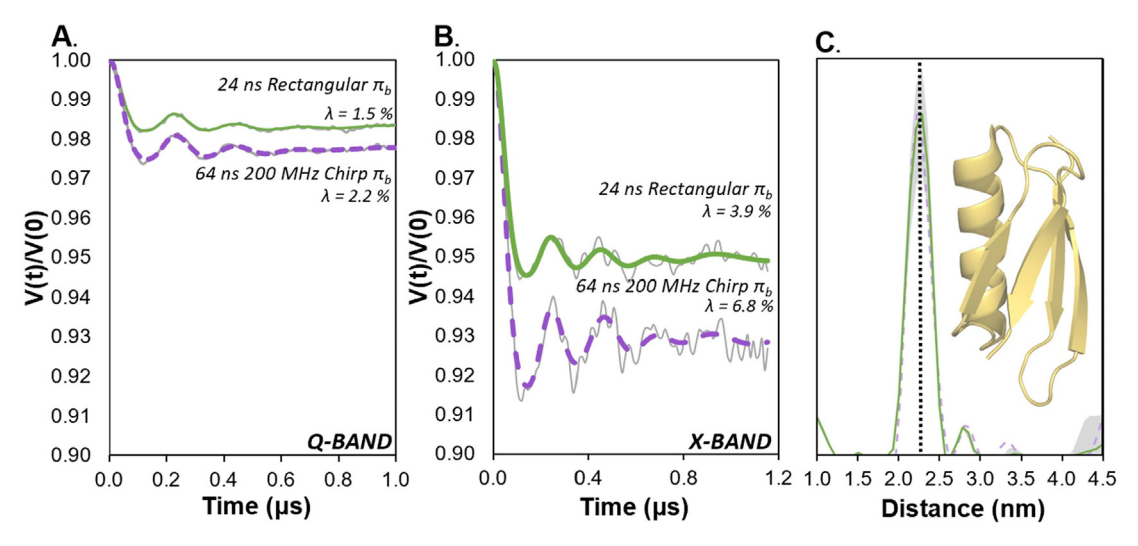


Fig. 7. Background subtracted DEER time traces (grey) collected from GB1 mutant 15H/17H/28H/32H at both A) Q-Band and B) X-Band. Time trace fits (green and purple) were obtained by DEERAnalysis2019 via Tikhonov regularization. The pump pulse utilized for each time trace is shown. Although the chirp pump pulse is truncated due to the shorter dipolar period of expected distance, there is still a notable gain in modulation depth ( $\lambda$ ). C) Validated Cu(II)-Cu(II) distance measurements comparison of X-Band distributions obtained using a rectangular (green) and 64 ns 200 MHz chirp pulse (purple). The distributions remain similar regardless of the pump pulse used. The grey shadow region shows the validated distributions from DEERAnalysis2019. The crystal structure of GB1 (PDB: 2J52) is shown. (For interpretation of the references to colour in this figure legend, the reader is referred to the web version of this article.)

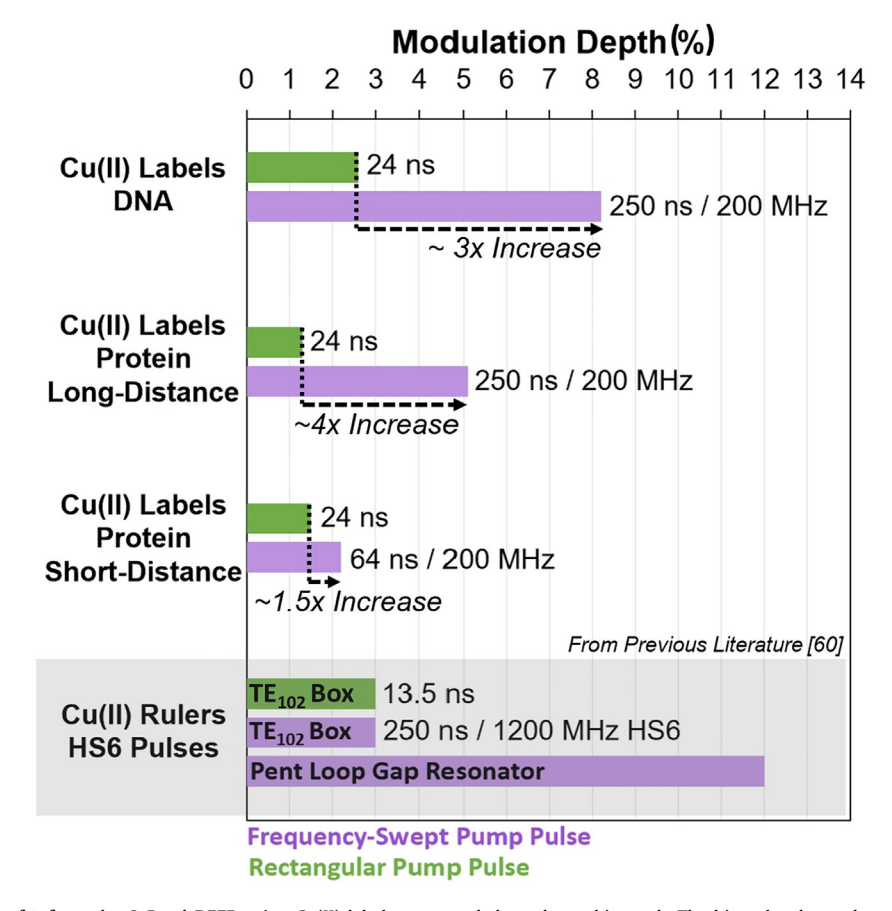


Fig. 8. Histogram comparison of  $\lambda$  from the Q-Band DEER using Cu(II) labels presented throughout this work. The biomolecules and pump pulse for each data set are described. The  $\lambda$  for Cu(II) rulers are from a previous study and presented here as an additional comparison to our work. The resonators and pump pulse used to obtain the Cu (II) ruler data are shown [60]. All data presented were collected on a commercial spectrometer.

we anticipate these results are reproducible if adapted under similar spectrometer setups using samples efficiently spin labeled with Cu(II). However as shown, further improvements can be made

using ultra-wide band pulses and a pent loop gap resonator. Notably, these significant sensitivity increases with chirp pulses can

reduce measurement collection time from a day to only a few hours.

### 3.8. Long-range distance measurements with chirp pulses can be obtained in a few hours

Next, we wanted to demonstrate the reduction in measurement collection times due to the increased sensitivities from the chirp pulse. To this end, the Q-Band time traces on Cu(II) spin labeled hGSTA1-1 liganded with GSHex (c.f. Fig. 6A) were obtained at different collection times. The time traces were collected until an SNR of 20 was achieved for the averaged background subtracted time trace. An SNR of 20 was chosen as our DEER sensitivity benchmark

minimum based on recently published EPR community guidelines for reporting distance distributions [98].

Fig. 9A shows that 30 mins of data collection at each field is sufficient to obtain an averaged time trace with an SNR of 20. It is clear from the data that long-range Cu(II)-Cu(II) distance measurements can be completed in less than two hours for protein concentrations on the order of 75  $\mu M$ . However, these collection times can vary since the time between measurements is usually dependent on the longitudinal relaxation time of Cu(II). For optimal sensitivity Cu(II) measurements are conventionally carried out at a temperature that minimizes the ratio between longitudinal and spin phase memory relaxation times [61]. With respect to the labels used in this work, we have previously shown that spin concentrations up to 800  $\mu M$  and temperatures between 18 and 20 K have an invari-

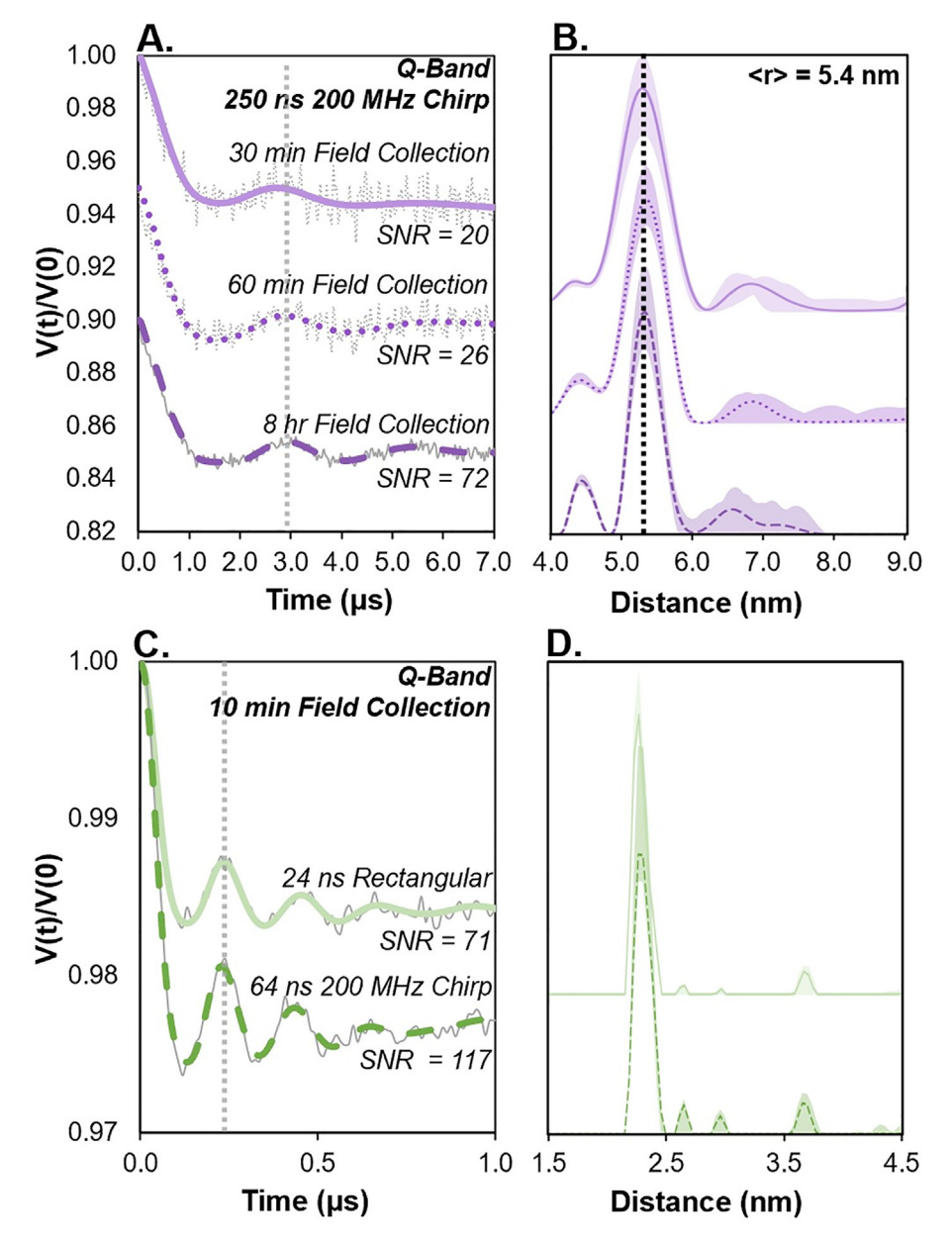


**Fig. 9.** A) Background subtracted orientationally averaged DEER time traces obtained from Cu(II) spin labeled E211H/K215H hGSTA1-1 liganded with GSHex. Each DEER is summed at various collection times as shown. The y-axis values are staggered for easier comparison of the time traces. After 30 mins of collecting each field (1.5 hrs total) the final DEER time trace reaches the minimum SNR of 20 for distance distribution analysis. B) Distance distribution comparison for each of the final time traces summed with respect to collection time. C) Summation of the three dHis + Cu(II)-NTA GB1 Q-band orientationally selective DEER time traces collected for 10 mins each with pump pulses as shown D) Distance distribution comparison obtained from the time trace summations for rectangular (solid) and chirp pulse (dashed) pump pulses. The shaded region represents the validated distributions from DEERAnalysis2019.

ant effect on the ratio of relaxation times [73]. Nevertheless, improvements to the SNR are easily made as needed with longer collection times. For example, the time trace from Fig. 9A with an SNR of 72 was acquired in only a day. Note that the time trace SNR does not increase as root function with respect to collection time since it is a weighted sum of measurements collected at different magnetic fields. Fig. 9B shows the distance distribution at three collection times. It is evident that the most probable distances are in good agreement, but there is a small difference in the breadth of the distributions.

We then carried out the collection time analysis with respect to short-range distance measurements on Cu(II) spin labeled GB1 (c.f. Fig. S7). Fig. 9C shows that collecting each field measurement for 10 mins provides summed time traces with SNR exceeding 20. Indeed, it took only 30 mins of collection time with either pump pulse to complete the measurement. The minimum collection time was 10 mins at each magnetic field due to the tau averaging cycle used to suppress ESEEM contributions to the DEER signal (c.f. Methods and Experimental). Further, Fig. 8D shows the distance distributions obtained using either pump pulse have no distinct differences.

### 4. Conclusion

In summary we have shown chirp pulses accessible with commercial instrumentation can provide significant gains in DEER sensitivity for Cu(II) spin pairs. The sensitivities improved 3 to 4 times at both X and O-Band frequencies. Indeed, modulation depths of 18 % can be obtained utilizing commercial instrumentation at X-band, leading to significant reduction in collection times. For example, we show that a 7 µs DEER on Cu(II) protein labels that require multiple measurements can be completed in under 2 hrs. Such an achievement is exciting since it was only recently that time traces exceeding  $\sim 4 \,\mu s$  became practical to obtain using Cu(II) labels [73]. Additionally, we show that our commercial instrumentation setup provides modulation depths that are comparable with previous measurements that used custom pent loop gap resonators and ultra-wide band pulses. Even though only two Cu(II) spin labels were presented in this work as example cases, we anticipate our results are widely applicable to other systems that contain endogenous Cu(II). Further improvements to this work can be made by probing a wider range of the Cu(II) spectrum using an AWG suitable for ultra-wideband pulse [60]. In addition, replacing the DEER observer pulses with shaped chirp pulses can further improve sensitivity [60]. Cumulatively this work presents a systematic sensitivity comparison to demonstrate the robustness of Cu(II) spin label technology with commercial EPR equipment.

### Data availability

Data will be made available on request.

### **Declaration of Competing Interest**

The authors declare that they have no known competing financial interests or personal relationships that could have appeared to influence the work reported in this paper.

### Acknowledgements

This research was funded by the National Science Foundation (NSF BSF MCB-2006154). All MD Simulations were carried out at the University of Pittsburgh Center for Research Computing. We would also like to thank Ina Garten for reminding us that if you do not wish make it from scratch, then "store-bought is fine".

### Appendix A. Supplementary material

Supplementary data to this article can be found online at https://doi.org/10.1016/i.imr.2023.107413.

#### References

- [1] O. Schiemann, T.F. Prisner, Long-Range Distance Determinations in Biomacromolecules by EPR Spectroscopy, Q. Rev. Biophys. 40 (2007) 1–53.
- [2] L.J. Berliner, G.R. Eaton, S.S. Eaton, Distance Measurements in Biological Systems by EPR, first ed., Springer, New York, New York, 2000.
- [3] A.D. Milov, A.G. Maryasov, Y.D. Tsvetkov, Pulsed electron double resonance (PELDOR) and its applications in free-radicals research, Appl. Magn. Reson. 15 (1998) 107–143.
- [4] M. Bonora, J. Becker, S. Saxena, Suppression of electron spin-echo envelope modulation peaks in double quantum coherence electron spin resonance, J. Magn. Reason. 170 (2004) 278–283.
- [5] S. Milikisyants, F. Scarpelli, M.G. Finiguerra, M.H. Ubbink, M.A Pulsed EPR Method to determine distances between paramagnetic centers with strong spectral anisotropy and radicals: the dead-time free RIDME sequence, J. Magn. Reson. 201 (2009) 48–56.
- [6] G. Jeschke, M. Pannier, A. Godt, H.W. Spiess, Dipolar spectroscopy and spin alignment in electron paramagnetic resonance, Chem. Phys. Lett. 331 (2000) 243–252.
- [7] P.P. Borbat, J.H. Freed, Multiple-quantum ESR and distance measurements, Chem. Phys. Lett. 313 (1999) 145–154.
- [8] L.V. Kulik, S.A. Dzuba, I.A. Grigoryev, Y.D. Tsvetkov, Electron dipole-dipole interaction in ESEEM of nitroxide biradicals, Chem. Phys. Lett. 343 (2001) 315– 324
- [9] T. Schmidt, M.A. Wälti, J.L. Baber, E.J. Hustedt, G.M. Clore, Long distance measurements up to 160 Å in the GroEL tetradecamer using Q-Band DEER EPR spectroscopy, Angew. Chem. Int. Ed. 55 (2016) 15905–15909.
- [10] G. Jeschke, DEER distance measurements on proteins, Ann. Rev. Phys. Chem. 63 (2012) 419–446
- [11] I. Krstić, B. Endeward, D. Margraf, A. Marko, T.F. Prisner, Structure and dynamics of nucleic acids, Top. Curr. Chem. 321 (2012) 159–198.
- [12] C. Altenbach, A.K. Kusnetzow, O.P. Ernst, K.P. Hofmann, W.L. Hubbell, Highresolution distance mapping in rhodopsin reveals the pattern of helix movement due to activation, Proc. Natl. Acad. Sci. 105 (2008) 7439–7444.
- [13] L. Galazzo, G. Meier, M. Hadi Timachi, C.A.J. Hutter, M.A. Seeger, E. Bordignon, Spin-labeled nanobodies as protein conformational reporters for electron paramagnetic resonance in cellular membranes, Proc. Natl. Acad. Sci. 117 (2020) 2441–2448.
- [14] E.G.B. Evans, J.L.W. Morgan, F. DiMaio, W.N. Zagotta, S. Stoll, Allosteric conformational change of a cyclic nucleotide-gated ion channel revealed by DEER spectroscopy, Proc. Natl. Acad. Sci. 117 (2020) 10839–10847.
- [15] R. Dastvan, A. Rasouli, S. Dehghani-Ghahnaviyeh, S. Gies, E. Tajkhorshid, Proton-driven alternating access in a spinster lipid transporter, Nat. Commun. 131 (2022) 1–15.
- [16] J. Casto, A. Mandato, L. Hofmann, I. Yakobov, S. Ghosh, S. Ruthstein, S. Saxena, Cu(II)-Based DNA labeling identifies the structural link between transcriptional activation and termination in a metalloregulator, Chem. Sci. 13 (2022) 1693–1697.
- [17] K.M. Stone, J.E. Townsend, J. Sarver, P.J. Sapienza, S. Saxena, L. Jen-Jacobson, Electron spin resonance shows common structural features for different classes of EcoRI-DNA complexes, Angew. Chem. Int. Ed. 47 (2008) 10192– 10194.
- [18] N.S. Tangprasertchai, R. Di Felice, X. Zhang, I.M.V. Slaymaker, C. Reyes, W. Jiang, R. Rohs, P.Z. Qin, CRISPR-Cas9 mediated DNA unwinding detected using site-directed spin labeling, ACS Chem. Biol. 12 (2017) 1489–1493.
- [19] H. Sameach, S. Ruthstein, EPR distance measurements as a tool to characterize protein-DNA interactions, Isr. J. Chem. 59 (2019) 980–989.
- [20] C. Wuebben, M.F. Vicino, M. Mueller, O. Schiemann, Do the P1 and P2 hairpins of the guanidine-II riboswitch interact?, Nucleic Acids Res 48 (2020) 10518– 10526.
- [21] D. Abdullin, N. Florin, G. Hagelueken, O. Schiemann, EPR-based approach for the localization of paramagnetic metal ions in biomolecules, Angew. Chem. Int. Ed. 54 (2015) 1827–1831.
- [22] A. Gamble Jarvi, T.F. Cunningham, S. Saxena, Efficient localization of a native metal ion within a protein by Cu<sup>2+</sup>-based EPR distance measurements, Phys. Chem. Chem. Phys. 21 (2019) 10238–10243.
- [23] G.L. Millhauser, Copper and the prion protein: methods, structures, function, and disease, Ann. Rev. Physc. Chem. 58 (2007) 299–320.
- [24] S.L. Meichsner, Y. Kutin, M. Kasanmascheff, In-cell characterization of the stable tyrosyl radical in *E. Coli* ribonucleotide reductase using advanced EPR spectroscopy, Angew. Chem. Int. Ed. 60 (2021) 19155–19161.
- [25] K. Ackerman, J.L. Wort, B.E. Bode, Pulse dipolar EPR for determining nanomolar binding affinities, Chem. Comm. 58 (2022) 8790–8793.
- [26] T. Schmidt, J. Jeon, W. Yau, C.D. Scheieters, R. Tycko, G.M. Clore, Time-resolved DEER EPR and solid-state NMR afford Kinect and structural elucidation of substrate binding to Ca2+-ligated calmodulin, Proc. Natl. Acad. Sci. 119 (2022), e2122308119
- [27] T. Hett, T. Zbik, S. Mukherjee, H. Matsuoko, W. Bönigk, D. Klose, C. Rouillon, N. Brenner, S. Peuker, R. Klement, H. Steinhoff, H. Grubmüller, R. Seifert, O.

- Schiemann, U.B. Kaupp, Spatiotemporal resolution of conformational changes in biomolecules by combining pulsed electron-electron double resonance spectroscopy with microsecond freeze-hyperquenching, J. Am. Chem. Soc. 143 (2021) 6981–6989.
- [28] S.J. Fries, T.S. Braun, C. Globisch, C. Peter, M. Drescher, E. Deuerling, Deciphering molecular details of the RAC-ribosome interaction by EPR spectroscopy, Sci. Reports. 11 (2021) 1–10.
- [29] H.S. McHaourab, P.R. Steed, K. Kazmier, Toward the fourth dimension of membrane protein structure: insight into dynamics from spin-labeling EPR spectroscopy, Structure 19 (2011) 1549–1561.
- [30] V. Singh, M. Azarkh, T.E. Exner, J.S. Hartig, M. Drescher, Human telomeric quadruplex conformations studied by pulsed EPR, Angew. Chem. Int. Ed. 48 (2009) 9728–9730.
- [31] B. Joseph, E.A. Jaumann, A. Sikora, K. Barth, T.F. Prisner, D.S. Cafiso, In situ observation of conformational dynamics and protein ligand-substrate interactions in outer-membrane proteins with DEER/PELDOR spectroscopy, Nat. Protoc. 14 (2019) 2344–2369.
- [32] B. Endeward, J.A. Butterwick, R. MacKinnon, T.F. Prisner, Pulsed electronelectron double-resonance determination of spin-label distances and orientations on the tetrameric potassium ion channel KcsA, J. Am. Chem. Soc. 131 (2009) 15246–15250.
- [33] K. Singewald, H. Hunter, T.F. Cunningham, S. Ruthstein, S. Saxena, Measurement of protein dynamics from site directed Cu(II) labeling, Anal. Sens. e203300053 (2022) 1–14.
- [34] W.L. Hubbell, C. Altenbach, Investigation of structure and dynamics in membrane proteins using site-directed spin labeling, Curr. Opin. Struct. Biol. 4 (1994) 566–573.
- [35] D.P. Claxton, M. Quick, L.D. Shi, F.D. Carvalho, H. Weinstein, J.A. Javitch, H.S. McHaourab, Ion/Substrate-dependent conformational dynamics of a bacterial homolog of neurotransmitter: sodium symporters, Nat. Struct. Mol. Biol. 17 (2010) 822–829.
- [36] W.L. Hubbell, H.S. Mchaourab, C. Altenbach, M.A. Lietzow, Watching proteins move using site-directed spin labeling, Struct. 4 (1996) 779–783.
- [37] W.L. Hubbell, C.J. López, C. Altenbach, Z. Yang, Technological advances in sitedirected spin labeling of proteins, Curr. Opin. Struct. Bio. 23 (2013) 725-733.
- [38] Q. Cai, A.K. Kusnetzow, W.L. Hubbell, I.S. Haworth, G.P.C.V. Gacho, N. Eps, K. Hideg, E.J. Chambers, P.Z. Qin, Site-directed spin labeling measurements of nanometer distances in nucleic acids using a sequence-independent nitroxide probe, Nucleic Acids Res. 34 (2006) 4722–4730.
- [39] O. Schiemann, N. Piton, J. Plackmeyer, B.E. Bode, T.F. Prisner, J.W. Engels, Spin labeling of oligonucleotides with the nitroxide TPA and use of PELDOR, a pulse EPR method, to measure intramolecular distances, Nat. Protoc. 2 (2007) 904– 923
- [40] G.E. Fanucci, D.S. Cafiso, Recent advances and applications of site-directed spin labeling, Curr. Opin. Struct. Biol. 16 (2006) 644–653.
- [41] D.M. Engelhard, A. Meyer, A. Berndhäuser, O. Schiemann, G.H. Clever, Di-Copper(li) DNA G-quadruplexes as EPR distance rulers, Chem. Commun. 54 (2018) 7455–7458.
- [42] D. Goldfarb, Gd3+ Spin labeling for distance measurements by pulse EPR spectroscopy, Phys. Chem. Chemi. Phys. 16 (2014) 9685–9699.
- [43] A. Martorana, G. Bellapadrona, A. Feintuch, E.D. Gregorio, S. Aime, D. Goldfarb, Probing protein conformation in cells by EPR distance measurements using Gd3+ spin labeling, J. Am. Chem. Soc. 136 (2014) 13458–13465.
- [44] M. Qi, A. Groß, G. Jeschke, A. Godt, M. Drescher, Gd(III)-PyMTA Label Is suitable for in-Cell EPR, J. Am. Chem. Soc. 136 (2014) 15366–15378.
- [45] Z. Hasanbasri, K. Singewald, T.D. Gluth, B. Driesschaert, S. Saxena, Cleavageresistant protein labeling with hydrophilic trityl enables distance measurements in-cell, J. Phys. Chem. B. 125 (2021) 5265–5274.
- [46] G.Y. Shevelev, O.A. Krumkacheva, A.A. Lomzov, A.A. Kuzhelev, O.Y. Rogozhnikova, D.V. Trukhin, T.I. Troitskaya, V.M. Tormyshev, M.V. Fedin, D.V. Pyshnyi, E.G. Bagryanskaya, Physiological-temperature distance measurement in nucleic acid using triarylmethyl-based spin labels and pulsed dipolar EPR spectroscopy, J. Am. Chem. Soc. 136 (2014) 9874–9877.
- [47] M. Poncelet, B. Driesschaert, M. Poncelet, B. Driesschaert, A 13C-Labeled triarylmethyl radical as an EPR spin probe highly sensitive to molecular tumbling, Angew. Chem. Int. Ed. 59 (2020) 16451–16454.
- [48] N. Fleck, C. Heubach, T. Hett, S. Spicher, S. Grimme, O. Schiemann, Ox-SLIM: synthesis of and site-specific labelling with a highly hydrophilic trityl spin label, Chem. Eur. J. 27 (2021) 5292–5297.
- [49] D. Abdullin, O. Schiemann, Pulsed dipolar EPR spectroscopy and metal ions: methodology and biological applications, ChemPlusChem 85 (2020) 353–372.
- [50] E.P. Wagner, K.C. Gronborg, S. Ghosh, S. Saxena, An undergraduate experiment to explore Cu(II) coordination environment in multihistidine compounds through electron spin resonance spectroscopy, J. Chem. Educ. 96 (2019) 1752– 1759.
- [51] M. Pannier, S. Veit, A. Godt, G. Jeschke, H.W. Spiess, Dead-time free measurement of dipole-dipole interactions between electron spins, J. Magn. Reson. 142 (2000) 331–340.
- [52] X. Bogetti, S.G. Ghosh, A. Jarvi, J. Wang, S. Saxena, Molecular dynamics simulations based on newly developed force field parameters for Cu2+ spin labels provide insights into double-histidine-based double electron-electron resonance, J. Phys. Chem. B. 124 (2020) 2788–2797.
- [53] A. Gamble Jarvi, K. Ranguelova, S. Ghosh, R.T. Weber, S. Saxena, On the use of Q-band double electron-electron resonance to resolve the relative orientations of two double histidine-bound Cu2+ ions in a protein, J. Phys. Chem. B. 122 (2018) 10669–10677.

- [54] D. Idiyatullin, C. Corum, J.Y. Park, M. Garwood, Fast and quiet MRI using a swept radiofrequency, J. Magn. Reson. 181 (2006) 342–349.
- [55] E. Kupče, R. Freeman, An adaptable NMR broadband decoupling scheme, Chem. Phys. Lett. 250 (1996) 523–527.
- [56] P.E. Spindler, P. Schöps, W. Kallies, S.J. Glaser, T.F. Prisner, Perspectives of shaped pulses for EPR spectroscopy, J. Magn. Reson. 280 (2017) 30–45.
- [57] A. Doll, G. Jeschke, Wideband frequency-swept excitation in pulsed EPR spectroscopy, J. Magn. Reson. 280 (2017) 46-62.
- [58] C.E. Tait, S. Stoll, Coherent pump pulses in double electron electron resonance spectroscopy, Phys. Chem. Chem. Phys. 18 (2016) 18470–18485.
- [59] I. Kaminker, R. Barnes, S. Han, Arbitrary waveform modulated pulse EPR at 200 GHz, J. Magn. Reson. 279 (2017) 81–90.
- [60] F.D. Breitgoff, K. Keller, M. Qi, D. Klose, M. Yulikov, A. Godt, G. Jeschke, UWB DEER and RIDME distance measurements in Cu(II)–Cu(II) spin pairs, J. Magn. Reson. 308 (2019) 106560.
- [61] A. Doll, S. Pribitzer, R. Tschaggelar, G. Jeschke, Adiabatic and fast passage ultrawideband inversion in pulsed EPR, J. Magn. Reson. 230 (2013) 27–39.
- [62] T. Bahrenberg, Y. Rosenski, R. Carmieli, K. Zibzener, M. Qi, V. Frydman, A. Godt, D. Goldfarb, A. Feintuch, Improved sensitivity for W-band Gd(III)-Gd(III) and nitroxide-nitroxide DEER measurements with shaped pulses, J. Magn. Reson. 283 (2017) 1–13.
- [63] A. Giannoulis, K. Ackermann, P.E. Spindler, C. Higgins, D.B. Cordes, A.M.Z. Slawin, T.F. Prisner, B.E. Bode, Nitroxide-nitroxide and nitroxide-metal distance measurements in transition metal complexes with two or three paramagnetic centres give access to thermodynamic and kinetic stabilities, Phys. Chem. Chem. Phys. 20 (2018) 11196–11205.
- [64] P. Schöps, P.E. Spindler, A. Marko, T.F. Prisner, Broadband spin echoes and broadband SIFTER in EPR, J. Magn. Reson. 250 (2015) 55–62.
- [65] A. Doll, M. Qi, A. Godt, G. Jeschke, CIDME: short distances measured with long chirp pulses, J. Magn. Reson. 272 (2016) 73–82.
- [66] R. Tschaggelar, F.D. Breitgoff, O. Oberhänsli, M. Qi, A. Godt, G. Jeschke, Highbandwidth Q-band EPR resonators, Appl. Magn. Reson. 48 (2017) 1273–1300.
- [67] T.F. Segawa, A. Doll, S. Pribitzer, G. Jeschke, Copper ESEEM and HYSCORE through ultra-wideband chirp EPR spectroscopy, J. Chem. Phys. 143 (2015) 044201
- [68] I. Ritsch, H. Hintz, G. Jeschke, A. Godt, M. Yulikov, Improving the accuracy of Cu (II)-nitroxide RIDME in the presence of orientation correlation in watersoluble Cu(II)-nitroxide rulers, Phys. Chem. Chem. Phys. 21 (2019) 9810–9830.
- [69] A. Gamble Jarvi, X. Bogetti, K. Singewald, S. Ghosh, S. Saxena, Going the DHistance: site-directed Cu2+labeling of proteins and nucleic acids, Acc. Chem. Res. 54 (2021) 1481–1491.
- [70] M.J. Lawless, J.R. Pettersson, G.S. Rule, F. Lanni, S. Saxena, ESR resolves the C terminus structure of the ligand-free human glutathione S-transferase A1–1, Biophys. J. 114 (2018) 592–601.
- [71] S. Ghosh, M.J. Lawless, G.S. Rule, S. Saxena, The Cu2+-nitrilotriacetic acid complex improves loading of α-helical double histidine site for precise distance measurements by pulsed ESR, J. Magn. Reson. 286 (2018) 63–171.
- [72] A. Gamble Jarvi, J. Casto, S. Saxena, Buffer effects on site directed Cu2+-labeling using the double histidine motif, J. Magn. Reson. 320 (2020) 106848.
- [73] J. Casto, A. Mandato, S. Saxena, DHis-troying barriers: deuteration provides a pathway to increase sensitivity and accessible distances for Cu2+ labels, J. Phys. Chem. Lett. 12 (2021) 4681–4685.
- [74] K. Singewald, J.A. Wilkinson, S. Saxena, Copper based site-directed spin labeling of proteins for use in pulsed and continuous wave EPR spectroscopy, Bio-protocol, 11 (2021) e4258.
- [75] T.F. Cunningham, S. Pornsuwan, W.S. Horne, S. Saxena, Rotameric preferences of a protein spin label at edge-strand  $\beta$ -sheet sites, Protein Sci. 25 (2016) 1049–1060.
- [76] T.F. Cunningham, M.S. McGoff, I. Sengupta, C.P. Jaroniec, W.S. Horne, S. Saxena, High-resolution structure of a protein spin-label in a solvent-exposed β-sheet and comparison with DEER spectroscopy, Biochem. 51 (2012) 6350–6359.
- [77] S. Stoll, A. Schweiger, EasySpin, a comprehensive software package for spectral simulation and analysis in EPR, J. Magn. Reson. 178 (2006) 42–55.
- [78] S.G. Worswick, J.A. Spencer, G. Jeschke, I. Kuprov, Deep neural network processing of DEER data, Sci. Adv. 4 (2018) eaat5218.
- [79] G. Jeschke, V. Chechik, P. Ionita, A. Godt, H. Zimmermann, J. Banham, C.R. Timmel, D. Hilger, H. Jung, DeerAnalysis2006 a comprehensive software package for analyzing pulsed ELDOR data, App. Mag. Reason. 30 (2006) 473–498.
- [80] M.J. Lawless, J.L. Sarver, S. Saxena, Nucleotide-independent Copper(II)-based distance measurements in DNA by pulsed ESR spectroscopy, Angew. Chem. Int. Ed. 56 (2017) 2115–2117.
- [81] S. Ghosh, J. Casto, X. Bogetti, C. Arora, J. Wang, S. Saxena, Orientation and dynamics of Cu2+ based DNA labels from force field parameterized MD elucidates the relationship between EPR distance constraints and DNA backbone distances, Phys. Chem. Chem. Phys. 22 (2020) 26707–26719.
- [82] S. Ghosh, M.J. Lawless, H.J. Brubaker, K. Singewald, M.R. Kurpiewski, L. Jen-Jacobson, S. Saxena, Cu2+-Based distance measurements by pulsed EPR provide distance constraints for DNA backbone conformations in solution, Nucleic Acids Res. 48 (2020) e49.
- [83] Z. Yang, D. Kise, S. Saxena, An Approach towards the measurement of nanometer range distances based on Cu2+ ions and ESR, J. Phys. Chem. B. 114 (2010) 6165–6174.
- [84] H. Ghimire, R.M. Mccarrick, D.E. Budil, G.A. Lorigan, Significantly improved sensitivity of Q-Band PELDOR/DEER experiments relative to X-band Is

- observed in measuring the intercoil distance of a leucine zipper motif peptide (GCN4-LZ), Biochem. 48 (2009) 5782–5784.
- [85] T.F. Prisner, M. Rohrer, F. Macmillan, Pulsed EPR spectroscopy: biological applications, Ann. Rev. Phys. Chem. 52 (2001) 279–313.
- [86] B.E. Bode, D. Margraf, J. Plackmeyer, G. Dürner, T.F. Prisner, O. Schiemann, Counting the monomers in nanometer-sized oligomers by pulsed electron–electron double resonance, J. Am. Chem. Soc. 129 (2007) 6736–6745.
- [87] D. Abdullin, P. Brehm, N. Fleck, S. Spicher, S. Grimme, O. Schiemann, Pulsed EPR dipolar spectroscopy on spin pairs with one highly anisotropic spin center: THE low-spin FellI Case, Chem. Eur. J. 25 (25) (2019) 14388–14398.
- [88] Z. Hasanbasri, M. Ponclet, H.R. Hunter, B. Driesschaert, S. Saxena, A new <sup>13</sup>C trityl-based spin label enables the use of DEER for distance measurements, J. Magn. Reson. 347 (2023) 10763, https://doi.org/10.1016/j.jmr.2022.107363, In Press
- [89] Y. Zhan, G.S. Rule, Glutathione induces helical formation in the carboxy terminus of human glutathione transferase A1–1, Biochem. 43 (2004) 7244– 7254.
- [90] E. Grahn, M. Novotny, E. Jakobsson, A. Gustafsson, L. Grehn, B. Olin, D. Madsen, M. Wahlberg, B. Mannervik, G.J. Kleywegt, New crystal structures of human glutathione transferase A1–1 shed light on glutathione binding and the conformation of the C-terminal helix, Acta Cryst. D 62 (2006) 197–207.
- [91] M.J. Lawless, S. Ghosh, T.F. Cunningham, A. Shimshi, S. Saxena, On the use of the Cu2+-iminodiacetic acid complex for double histidine based distance

- measurements by pulsed ESR, Phys. Chem. Chem. Phys. 19 (2017) 20959–20967.
- [92] H. Sameach, S. Ghosh, L. Gevorkyan-Airapetov, S. Saxena, S. Ruthstein, EPR spectroscopy detects various active state conformations of the transcriptional regulator CueR, Angew. Chem. Int. Ed. 58 (2019) 3053–3056.
- [93] S. Ghosh, S. Saxena, G. Jeschke, Rotamer modelling of Cu(II) spin labels based on the double-histidine motif, Appl. Magn. Reson. 49 (2018) 1281–1298.
- [94] T.F. Cunningham, M.R. Putterman, A. Desai, W.S. Horne, S. Saxena, The double-histidine Cu2+-binding motif: A highly rigid, site-specific spin probe for electron spin resonance distance measurements, Angew. Chem. Int. Ed. 54 (2015) 6330–6334.
- [95] X. Bogetti, Z. Hasanbasri, H.R. Hunter, S. Saxena, An optimal acquisition scheme for Q-Band EPR distance measurements using Cu2+-based protein labels, Phys. Chem. Chem. Phys. 24 (2022) 14727–14739.
- [96] J.L. Wort, K. Ackermann, D.G. Norman, B.E. Bode, A general model to optimise Cu(II) Labelling Efficiency of Double-Histidine Motifs for Pulse dipolar EPR applications, Phys. Chem. Chem. Phys. 23 (2021) 3810–3819.
- [97] J.L. Wort, S. Arya, K. Ackermann, A.J. Stewart, B.E. Bode, Pulse dipolar EPR reveals double-histidine motif Cu I –NTA spin-labeling robustness against competitor ions, J. Phys. Chem. Lett. 12 (2021) 2815–2819.
- [98] O. Schiemann et al., Benchmark test and guidelines for DEER/PELDOR experiments on nitroxide-labeled biomolecules, J. Am. Chem. Soc. 143 (2021) 17875–17890.